Asociación Argentina
de Mecánica Computacional

Mecánica Computacional Vol XXVIII, págs. 1453-1462 (artículo completo)
Cristian García Bauza, Pablo Lotito, Lisandro Parente, Marcelo Vénere (Eds.)
Tandil, Argentina, 3-6 Noviembre 2009

A GALERKIN BOUNDARY ELEMENT METHOD FOR STOKES FLOW AROUND BODIES WITH SHARP CORNERS AND EDGES

Jorge D'Elía, Laura Battaglia, Alberto Cardona and Mario A. Storti

Centro Internacional de Métodos Computacionales en Ingeniería (CIMEC), Instituto de Desarrollo Tecnológico para la Industria Química (INTEC), Universidad Nacional del Litoral - CONICET , Güemes 3450, 3000-Santa Fe, Argentina, e-mail: jdelia@intec.unl.edu.ar, lbattaglia@santafe-conicet.gov.ar, acardona@intec.unl.edu.ar, mstorti@intec.unl.edu.ar, web page: http://www.cimec.org.ar

Keywords: sharp corner, edge, double surface integral, Galerkin boundary element method, microhydrodynamics, three dimensional creeping flow.

Abstract. In this work, steady creeping three dimensional flow of a viscous and incompressible fluid around closed rigid bodies with sharp corners and edges is numerically solved using a Galerkin scheme applied to a modified Power-Miranda boundary integral equation. The related double surface integrals that account the pairwise interaction among all boundary elements are quadruple and they are computed on flat simplex triangles using the scheme proposed by Taylor (D. J. Taylor, IEEE Trans. on Antennas and Propagation, 51(7):1630–1637 (2003)). As a numerical example, the creeping steady flow around the unit cube considering different orientations with respect to the unperturbed fluid velocity, covering issues on the surface traction exponents close to the edges and vertices and compared against semi-analytical computations.

1 INTRODUCTION

Stokes flow around rigid bodies with sharp corners and edges are frequently encountered, among other applications, in Micro-Electro-Mechanical Systems (MEMS), e.g. see Wang (2002) or Méndez et al. (2008). As it is known, the presence of geometric discontinuities such as corners and edges is associated with the singular behavior of the stress and traction fields in both hydrodynamics and elasticity problems, e.g. see Kozlov et al. (2001).
The surface tractions at a sharp corner, such as a three dimensional (3D) vertex, are at least as singular as those encountered at the edges, since a point near the vertex of a polyhedral surface is also in the neighborhood of an edge. Nevertheless, Mustakis and Kim (1998) have already shown that boundary integral equation techniques can be appropiate for solving these flow cases.
In the present work, the Power and Miranda (1987) boundary integral equation is adapted for Stokes flow around rigid bodies with sharp corners and edges, and it is numerically solved using the so called Galerkin Boundary Element Method (GBEM) or Variational Boundary Element Method (VBEM), e.g. see Paquay (2002); D'Elía et al. (2008) with a full numerical quadrature of the related weakly singular double surface integrals (Taylor, 2003a; D'Elía et al., 2009).
As a sharp body, a unit cube is considered in the numerical examples, for which the traction coefficient close to the edges and corners are plotted, considering different orientations with respect to an unperturbed fluid velocity, covering issues on the surface traction exponents close to the edges and vertices with comparisons against semi-analytical computations.

2 GOVERNING EQUATIONS

For the creeping flow around a closed, rigid and piecewise smooth body surface S, the Power and Miranda (1987) alternative that allows the determination of a net force and torque on a closed body surface S by solving the modified boundary integral equation is written as

$$\int_S dS_{\mathbf{y}} \{\mathbf{K}[\boldsymbol{\psi}(\mathbf{x}) - \boldsymbol{\psi}(\mathbf{y})] + \mathbf{P}\boldsymbol{\psi}(\mathbf{y})\} = -\mathbf{u}(\mathbf{x}) \quad \text{for } \mathbf{x} \in S; \tag{1}$$

where $\boldsymbol{\psi}$ is a surface density potential and $\mathbf{u}(\mathbf{x})$ is the unperturbed incoming flow velocity. The differential element is denoted as $dS_{\mathbf{y}} = dS(\mathbf{y})$, while the integration and field points are $\mathbf{y} = (y_1, y_2, y_3)$ and $\mathbf{x} = (x_1, x_2, x_3)$, respectively.
The double-layer surface kernel $\mathbf{K} = \mathbf{K}(\mathbf{x}, \mathbf{y})$ is a tensor of rank 2. It is due to the surface density of stresslets over the body surface (Ladyzhenskaya, 1969; Pozrikidis, 1996, 1997), and it is given by

$$\begin{gathered} K_{ij}(\mathbf{x}, \mathbf{y}) = -\frac{3}{4\pi\mu} \frac{r_i\, r_j\, r_k}{r^5}\, n_k(\mathbf{y})\ ; \\ \text{with} \quad \mathbf{r} = \mathbf{x} - \mathbf{y} \quad \text{and } r = \|\mathbf{x} - \mathbf{y}\|_2; \end{gathered} \tag{2}$$

where μ is the dynamic fluid viscosity, while $n_k = n_k(\mathbf{y})$ is the unit surface normal at the integration point $\mathbf{y}$. For smooth surfaces, this kernel has the key property

$$\int_S dS_{\mathbf{y}} K_{ij}(\mathbf{x}, \mathbf{y}) = \frac{1}{2\mu}\delta_{ij} \qquad \text{for } \mathbf{x} \in S; \tag{3}$$

where δ_{ij} is the Kronecker delta.
The "sourcelet" kernel $\mathbf{P} = \mathbf{P}(\mathbf{x}, \mathbf{y})$ is due to stokeslet and rotlet sources although instead of the concentred ones at the body centroid, as in the original formulation of the Power and Miranda

(1987) alternative, in this work they are placed as surface source densities. In any case, they give rise to a force and a torque when the combined kernel is integrated over a closed surface that encloses it. Their approach is an extension to the steady Stokes equation of the Mikhlin results on the exterior Dirichlet problem for the Laplace equation (Mikhlin, 1965, 1970). A key idea of the Power-Miranda scheme is adopting the strength of the "sourcelet" kernel $\mathbf{P}$ linearly dependent upon the surface density potential $\boldsymbol{\psi}(\mathbf{y})$, i.e.,

$$\mathbf{P}(\mathbf{x},\mathbf{y}) = \mathbf{C}(\mathbf{x},\mathbf{y})\boldsymbol{\psi}(\mathbf{y}) \; ; \tag{4}$$

where the coupled matrix $\mathbf{C} = \mathbf{C}(\mathbf{x},\mathbf{y})$, after some algebra, can be written as

$$\mathbf{C} = \frac{1}{8\pi\mu R^3}\int_S dS_{\mathbf{y}}(\mathbf{S}+\mathbf{R}) \; ; \tag{5}$$

with its stokeslet part

$$\mathbf{S} = \begin{bmatrix} (r_1r_1+r^2) & r_1r_2 & r_1r_3 \\ r_2r_3 & (r_2r_2+r^2) & r_2r_3 \\ r_3r_1 & r_3r_2 & (r_3r_3+r^2) \end{bmatrix} \quad ; \tag{6}$$

and its rotlet one

$$\mathbf{R} = \begin{bmatrix} (r_2r_2+r_3r_3) & -r_1r_2 & -r_1r_3 \\ -r_2r_1 & (r_3r_3+r_1r_1) & -r_2r_3 \\ -r_3r_1 & -r_3r_2 & (r_1r_1+r_2r_2) \end{bmatrix} \; ; \tag{7}$$

since they are placed as surface layer densities instead of concentred ones. Reordering terms in Eq. (1),

$$\int_S dS_{\mathbf{y}}\{(\underbrace{\mathbf{P}-\mathbf{K}}_{\mathbf{A}})\boldsymbol{\psi}(\mathbf{y}) + \mathbf{K}\boldsymbol{\psi}(\mathbf{x})\} = -\mathbf{u}(\mathbf{x}) \quad \text{for } \mathbf{x}\in S; \tag{8}$$

that is

$$\int_S dS_{\mathbf{y}}\{\mathbf{A}\boldsymbol{\psi}(\mathbf{y}) + \mathbf{K}\boldsymbol{\psi}(\mathbf{x})\} = -\mathbf{u}(\mathbf{x}) \quad \text{for } \mathbf{x}\in S; \tag{9}$$

where $\mathbf{A} = \mathbf{A}(\mathbf{x},\mathbf{y})$ is the difference between both kernels $\mathbf{A} = \mathbf{P} - \mathbf{K}$. Then, the Power-Miranda alternative can be written as the boundary integral equation

$$\mathbf{I}(\mathbf{x};\boldsymbol{\psi}(\mathbf{x})) + \mathbf{u}(\mathbf{x}) = \mathbf{0} \quad \text{for } \mathbf{x}\in S; \tag{10}$$

with the integral operator

$$\mathbf{I}(\mathbf{x};\boldsymbol{\psi}(\mathbf{x})) = \int_S dS_{\mathbf{y}}\{\mathbf{A}\boldsymbol{\psi}(\mathbf{y}) + \mathbf{K}\boldsymbol{\psi}(\mathbf{x})\} \qquad \text{with } \mathbf{x}\in S; \tag{11}$$

where the solution field is the surface density potential $\boldsymbol{\psi}(\mathbf{x})$.

3 NUMERICAL FORMULATION

3.1 Surface density potential computation

It should be noted that Eq. (10) is an indirect boundary integral equation (Power and Wrobel, 1995; Kim and Karrila, 1989) since it does not give directly the surface traction. Instead, a

surface density potential is obtained. In this work, this boundary integral equation is numerically solved using a Galerkin technique (Paquay, 2002; D'Elía et al., 2008). On the other hand, a numerical computation of Eq. (11) by a Galerkin procedure involves the computation of double surface integrals with a weak singularity. Taylor (2003a,b) developed a systematic way for handling boundary meshes composed by flat triangules. The formulation is based on a convenient reordering of the four iterated integrations that moves the weak singularity to the origin of the four dimensional Euclidean real space (4D or $\mathbb{R}^4$) and, then, uses systematically the Duffy transformation (Duffy, 1982), i.e. regularizes the integrand by using polar coordinates. Thus, Taylor chooses a Gauss–Legendre numerical quadrature on three coordinates and makes an analytic integration in the fourth one. As this Taylor scheme is a bit restrictive since it is specific for wave propagation kernels in computational electromagnetics, a modification is proposed in D'Elía et al. (2009). The modification consists in a full numerical quadrature on the four coordinates in order to handle kernels with a weak singularity within a general framework.

3.2 Surface traction field computation

On one hand, the body force $\mathbf{F} = (F_x, F_y, F_z)$ and body torque $\tilde{\mathbf{F}} = (\tilde{F}_x, \tilde{F}_y, \tilde{F}_z)$ can be computed by the surface integrals (Power and Miranda, 1987)

$$\begin{aligned} \mathbf{F} &= \int_S dS_{\mathbf{y}} \boldsymbol{\psi} \; ; \\ \tilde{\mathbf{F}} &= \int_S dS_{\mathbf{y}} (\mathbf{r} \times \boldsymbol{\psi}) \; . \end{aligned} \tag{12}$$

On the other hand, the traction field $t_i(\mathbf{x})$ at the exterior of the closed surface S, is obtained using (Ladyzhenskaya, 1969)

$$t_i(\mathbf{x}) = -\frac{3}{4\pi} \int_S dS_{\mathbf{y}} \frac{r_i r_j r_k}{r^5} n_j(\mathbf{x}) \psi_k(\mathbf{y}) \quad \text{for } \mathbf{x} \in S; \tag{13}$$

where $\mathbf{r} = \mathbf{x} - \mathbf{y}$. It should be noted that Eq. (13) assumes that the unit normal $\mathbf{n}$ is well defined at the field point $\mathbf{x}$. This restriction precludes the use of this equation for the computation of the traction field at points with geometric discontinuities, as nodes, edges and vertex on the polyhedral surface mesh and, then, the panel centroids are employed as field points $\mathbf{x}$ in the numerical examples. Finally, the drag coefficients are computed as $K = F/(\mu U L)$ and $\tilde{K} = \tilde{F}/(\mu U L^2)$, as well as $K_x = F_x/(\mu U L)$ and $\tilde{K}_x = \tilde{F}_x/(\mu U L^2)$, where L is a typical length. Obviously, the body force obtained by summing the traction field given by Eq. (13) coincides with the one obtained with Eq. (12).

4 NUMERICAL EXAMPLE

4.1 Steady creeping flow around the unit cube

As it is known, steady creeping flow is restricted to fluid flow problems when the Reynolds numbers $\mathrm{Re} = UL/\nu$ are lower than one, where U and L are typical speed and length scales, while ν and $\mu = \rho\nu$ are the fluid kinematic and dynamic viscosities, respectively, and ρ is the fluid density.

As a sharp body, a unit cube is considered, whose center is placed at the origin in $\mathbb{R}^3$, see Fig. 1. The cube case is selected as a very crude simplification of MEMS geometries (Fachinotti et al., 2007). In the numerical simulations, the following values are adopted: fluid density

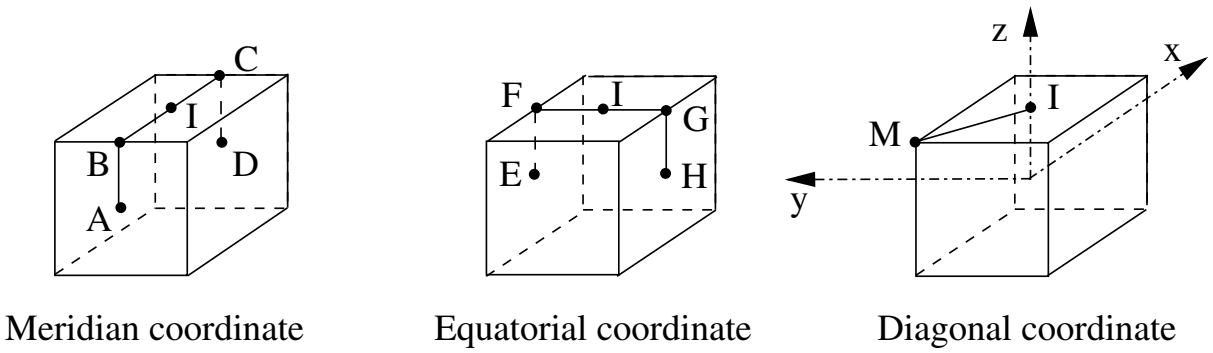

Figure 1: Meridian, equatorial and diagonal (poligonal) coordinates on the unit cube. The Cartesian coordinate system $O(x, y, z) = O(x_1, x_2, x_3)$ is centered.

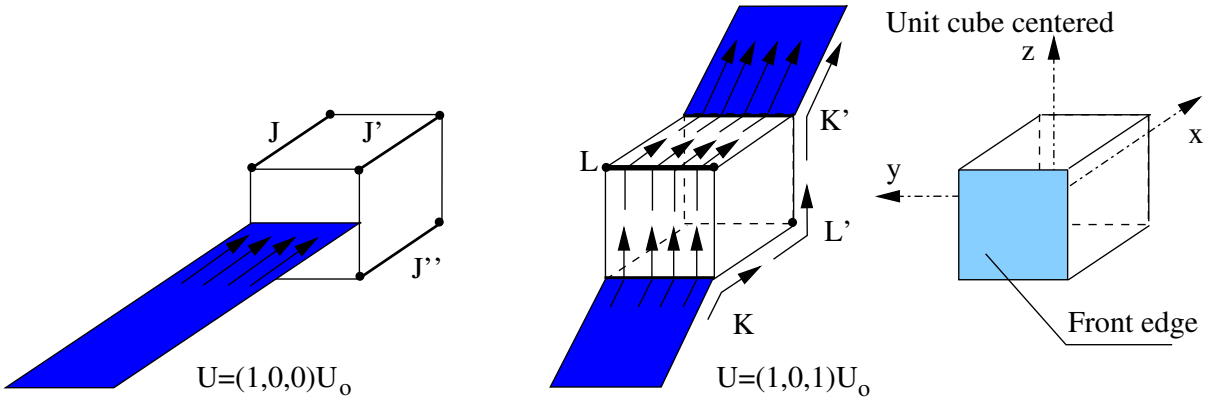

Figure 2: Two–dimensional Stokes flow modes across the middle of the edges of the unit cube: (i) parallel mode $\mathbf{U} = (1, 0, 0)U_0$, with parallel flow along edges J, J', J'' and J''' (not seen); (ii) splitting mode $\mathbf{U} = (1, 0, 1)U_0$, where the splitting edges K, K' have only the symmetric component while the L, L' edges have only the antisymmetric one, as given by Mustakis and Kim (1998), while U_0 is the unperturbed speed.

$\rho = 1$ kg/m^3, kinematic viscosity $\nu = 1$ m^2/s, incoming speed $U_0 = 0.001$ m/s and edge length $A = 1$ m. Thus, the typical length is $L = A = 1$ m.

There is no analytical solution in this case although bounds and semi numerical or experimental values are taken as a reference. For instance, an open interval bound is known for the drag force and it is given by $F_{\min} < F < F_{\max}$, with $F_{\min} = 3\pi\mu UA$ and $F_{\max} = \sqrt{3}F_{\min}$, where A is the cube edge length, or expressed as a drag coefficient interval, $K_{\min} < K < K_{\max}$, with $K_{\min} = 3\pi$ and $K_{\max} = 3\sqrt{3}\pi$.

On the other hand, following the work of Mustakis and Kim (1998), five modal flow problems are considered where, as a scaling in the fluid velocity is irrelevant, the incoming speed U_0 (a scalar) is introduced in the flow modes.

The first and second flow problems are the two–dimensional modes across the middle of the edges of the unit cube, as they are shown in Fig. 2: (i) the parallel mode $\mathbf{U} = (1, 0, 0)U_0$, with flow parallel to edges J, J', J'' and J''', see Fig. 2 (left), where J''' is not seen in this sketch; and (ii) the splitting mode $\mathbf{U} = (1, 0, 1)U_0$, where the edges K, K' and L, L' have to be considered, see Fig. 2 (center). The edges K and K' have the symmetric component, while the L and L' edges have the antisymmetric one, in such a way that each component has its own eigenvalue. The singularity exponents p were found by Mustakis/Kim as the solution to

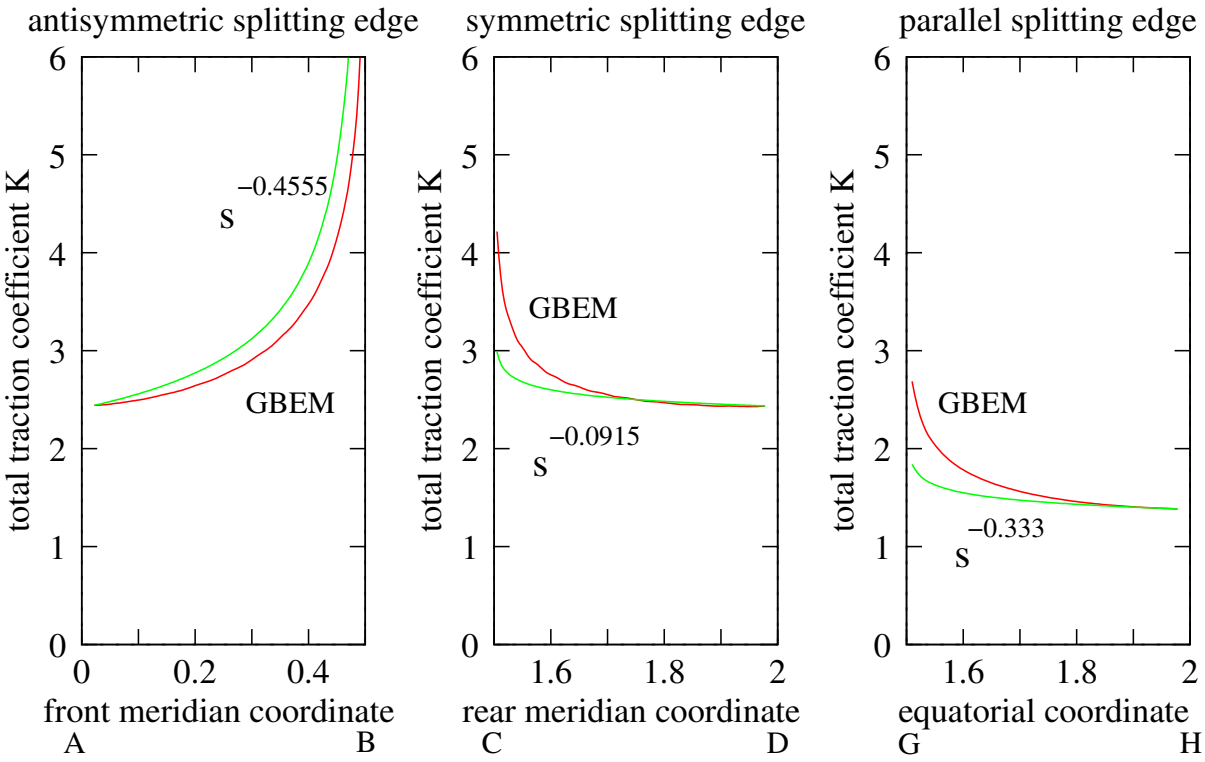

Figure 3: Two–dimensional Stokes flow modes across the middle of the edges of the unit cube. Total traction coefficients K as a function of the (poligonal) coordinates: front meridian AB (left), rear meridian CD (center), and equatorial GH (right). Comparison between a GBEM computation with the 6912 panel mesh and the semi-analytical asymptotic laws $O(s^p)$ (Mustakis and Kim, 1998), as a function of the distance s to the edge singularity. See Fig. 1, left and center, for the position of the points $A - H$.

an eigenvalue problem, giving, approximately, $\{-0.4555, -0.0915, -0.3333\}$, respectively, for each case.

The third, fourth and fifth flow problems are a symmetric and two antisymmetric 3D modes, respectively, not sketched in the figures. They are: symmetric with $\mathbf{U} = (1, 1, 1)U_0$, antisymmetric I with $\mathbf{U} = (1, 0, -1)U_0$, and antisymmetric II with $\mathbf{U} = (1, -2, 1)U_0$. The singularity exponents p for these were, approximately, $\{-0.31877, -0.62463\}$, respectively, i.e. the first eigenvalue for the symmetric mode and the second one for the two antisymmetric modes.

4.2 Solution with GBEM

The Gauss-Legendre quadrature formula is employed in the Taylor "black box" integrator, with $n_{1d} = 4$ Gauss–Legendre quadrature points in each coordinate for flat simplex triangles. Several GBEM meshes are used for solving this problem in order to check mesh convergence under refinement, although only results for $E = \{6912, 13\,872\}$ panel meshes are shown.

Semi-analytical asymptotic laws $O(s^p)$ for the total traction coefficients K, as a function of the distance s to the edge or vertex singularity, are given by Mustakis and Kim (1998). Comparisons between these and the present GBEM computation obtained with the 6912 panel mesh are shown in Figs. 3 and 4. It should be noted that Mustakis/Kim give only the traction law as a function of the distance s to the edge or vertex singularity and, then, only this dependence is checked in both figures.

For the two–dimensional Stokes flow modes across on the middle of the edges, the total traction coefficients K are plotted in Fig. 3 as a function of the (poligonal) coordinates: (i) front-

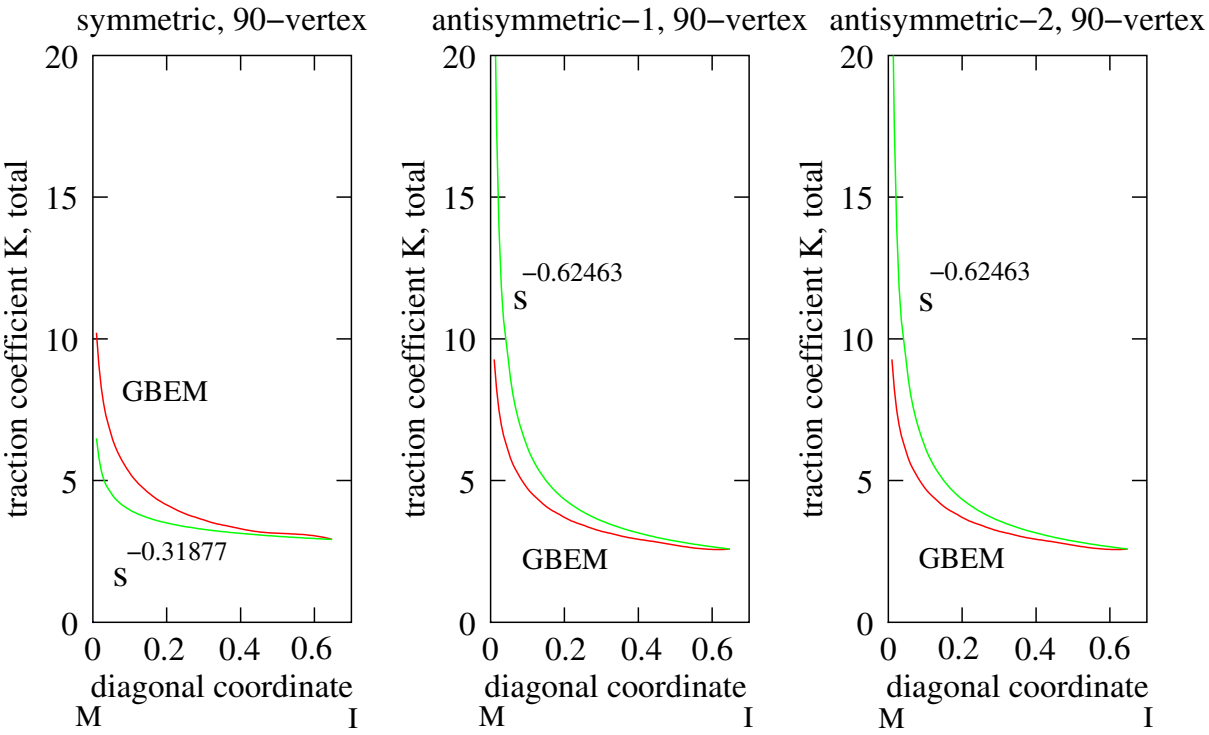

Figure 4: Three–dimensional Stokes flow modes of the 90 degree vertex of the unit cube. Total traction coefficients K as a function of the (poligonal) coordinate along the diagonal MI on the top plane. Comparison between a GBEM computation with the 6912 panel mesh and the semi-analytical asymptotic laws $O(s^p)$ (Mustakis and Kim, 1998), as a function of the distance s to the vertex singularity. See Fig. 1 (right), for the position of the points $M - I$.

meridian AB (left), rear-meridian CD (center), and equatorial GH (right). These (poligonal) coordinates are shown in Fig. 1 (left and center).

For the three–dimensional Stokes flow modes of the 90 degree vertex, the total traction coefficients K are plotted in Fig. 4 as a function of the (poligonal) coordinate along the diagonal MI (poligonal) coordinate on the top plane.

On the other hand, the parallel mode $U = (1, 0, 0)U_0$, with flow parallel to edges J, J', J'' and J''' which is shown in Fig. 3, gives the total traction coefficient in the x-Cartesian direction the value $K_x = 12.3879$, using the 13 872 panel mesh.

4.3 Solution with FEM

As another validation, a FEM computation had been performed with the open source PETSc-FEM code, which is a parallel multi-physics finite element library based on the Message Passing Interface (MPI, http://www.mpi-forum.org) and the Portable Extensible Toolkit for Scientific Computations (PETSc, http://www-fp.mcs.anl.gov/petsc). Among others applications of this solver are, for instance, free surface flows (D'Elía et al., 2002, 2000; Storti et al., 1998a,b), inertial waves in closed domains (D'Elía et al., 2006), and added mass computations (Storti and D'Elía, 2004). This code solves the Navier-Stokes equations with the SUPG/PSPG algorithm (Tezduyar et al., 1992; Sonzogni et al., 2000), i.e. using equal-order interpolations with the PSPG stabilization term in order to bypass the Brezzi-Babuska condition. The FEM computation does include the inertial terms, so that in order to compare with the GBEM results a low Reynolds number must be chosen.

The only flow case considered with a FEM computation is the parallel mode $\mathbf{U} = (1, 0, 0)U_0$,

with flow parallel to the edges J, J', J'' and J''', see Fig. 2 (left). The Reynolds number was set to 0.001 by choosing the particular combination of parameters $\nu = 0.1$, $U_\infty = 10^{-4}$ and $L = 1$. The flow is aligned with the x axis and, by symmetry, only one fourth of the domain ($y, z \geq 0$) was considered. The mesh was constructed by extrusion of a surface mesh having 50x50 quadrangles on each side of the cube, i.e. the mesh had $50 \times 50 \times 6/4 = 3750$ quadrangles on 1/4th of the cube inside a prismatic domain. The mesh spacing was non-uniform, with a logarithmic refinement towards the edges of the cube, where the results show that large friction values are found. This refinement was such that the linear size h of the quadrangles near the center of the face was in a ratio 5:1 to the size near the edges. This surface mesh was extruded in the radial direction into 50 layers of hexahedral elements in the radial direction from the cube surface, up to an external cube of length $L_{\text{ext}} = 50$. The width of layers in the radial direction were also refined towards the internal cube surface in such a way that the width of the external layer was in a ratio of 40:1 to the layer adjacent to the cube skin. Boundary conditions were velocity $\mathbf{u} = (U_\infty, 0, 0)$ at inlet ($x = -L_{\text{ext}}/2$), pressure $p = 0$ at outlet ($x = L_{\text{ext}}/2$), slip boundary condition at the lateral walls $y, z = \pm L_{\text{ext}}/2$, and non-slip boundary condition $\mathbf{u} = 0$ at the cube.

With this setup the computed value for the drag was $K = F_x/(\mu U_\infty L) = 13.76$. The numerical experiment was performed with other values of L_{ext} and mesh refinement in order to assess the sensibility of this result with respect to those parameters. This series of experiments have shown that this result is particularly sensitive to the size of the computational domain L_{ext}. This is so because the slip boundary conditions are equivalent to a lattice of mirrors of the cube with a spacing of $\Delta y = \Delta z = L_{\text{ext}}$. Then, each cube sees an *effective* external field given by U_∞ plus the velocity induced by the other cubes in the array. This field decays very slowly (as $O(1/L_{\text{ext}})$) for $L_{\text{ext}} \to \infty$, so that very large domains must be used in order to reduce the error. For instance, the error for $L_{\text{ext}} = 10$ is estimated in 15%. Computations for a sphere for which the drag can be computed analytically, show a similar behavior (D'Elía et al., 2008).

The traction map obtained with GBEM is close to the FEM one, while the traction coefficient is 10% lower than the FEM value. This difference deserves some comments. Both results fall within the interval $(K_{\min}, K_{\max})$ predicted by an analytic computation. In the GBEM computation the result is highly sensitive to the number of integration points, whereas for FEM the most influential parameter was the size of the computational domain. In both cases, some residual error may be due to insufficient mesh refinement. This is specially true in this case, because the strong variation of friction near the edges degrades the convergence with respect to mesh refinement. Figure 5 shows the Cartesian K_x component of the traction coefficient as a function of the meridian (poligonal) coordinate s_m (left), and as a function of the equatorial one s_e (right), obtained with FEM (solid line) and GBEM (cross) computation.

5 CONCLUSIONS

The singular behavior of the surface traction edges and corners in the tests cases solved in this work with a GBEM alternative is close to the singularity exponents obtained with a semi-analytical computation of Mustakis and Kim (1998). The present numerical solution of the surface traction near edges and corners has not shown numerical instabilities nor severe precision loss, although the traction field is somewhat regularized. Future work would be include the harmonic creeping flow case.

Acknowledgments This work has received financial support from Consejo Nacional de Investigaciones Científicas y Técnicas (CONICET, Argentina, grant PIP 5271–05), Universidad

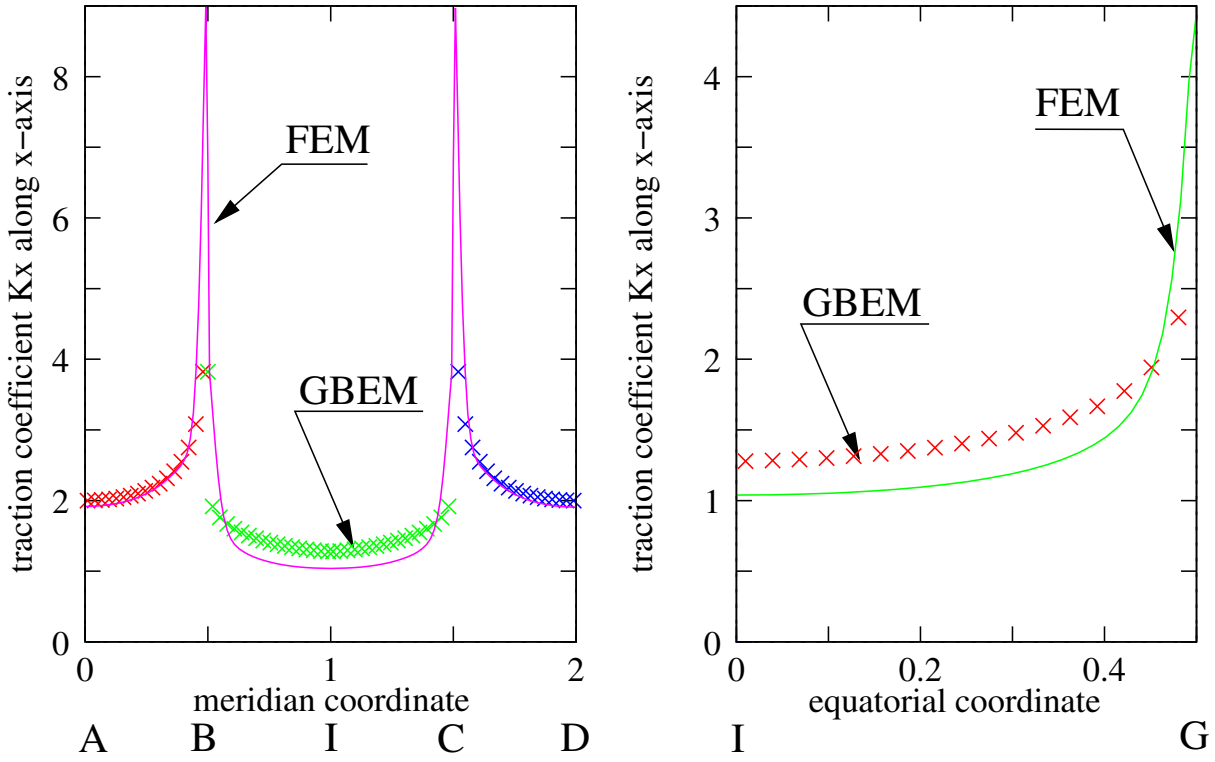

Figure 5: Cartesian K_x component of the traction coefficient as a function of the meridional and equatorial (poligonal) coordinates s_m (left) and s_e (right), with FEM (solid line) and GBEM (cross). See Fig. 1, left and center, for the position of the points $A - I$.

Nacional del Litoral (UNL, Argentina, grant CAI+D 2009–III-4–2), Agencia Nacional de Promoción Científica y Tecnológica (ANPCyT, Argentina, grants PICT 1506–06, PICT 1141–07 and PAE 22592–04 nodo 22961) and was performed with the *Free Software Foundation/GNU-Project* resources as GNU–Linux OS, GNU–Gfortran and GNU–Octave, as well as other Open Source resources as Scilab, TGif, Xfig and LaTeX.

REFERENCES

D'Elía J., Battaglia L., Cardona A., and Storti M. Full numerical quadrature of weakly singular double surface integrals in Galerkin boundary element methods. *Communications in Numerical Methods in Engineering*, 2009. In press.

D'Elía J., Battaglia L., Storti M., and Cardona A. Galerkin boundary integral equations applied to three dimensional Stokes flows. In Cardona, Storti, and Zuppa, editors, *Mecánica Computacional, vol. XXVII*, ISSN 1666–6070, pages 2397–2410. San Luis, 2008.

D'Elía J., Nigro N., and Storti M. Numerical simulations of axisymmetric inertial waves in a rotating sphere by finite elements. *International Journal of Computational Fluid Dynamics*, 20(10):673–685, 2006.

D'Elía J., Storti M., Oñate E., and Idelsohn S. A nonlinear panel method in the time domain for seakeeping flow problems. *Int. J. of Computational Fluid Dynamics*, 16(4):263–275, 2002.

D'Elía J., Storti M.A., and Idelsohn S.R. A panel-Fourier method for free surface methods. *ASME-Journal of Fluids Engineering*, 122(2):309–317, 2000.

Duffy M.G. Quadrature over a pyramid or cube of integrands with a singularity at a vertex. *SIAM Journal on Numerical Analysis*, 19(6):1260–1262, 1982.

Fachinotti V., Cardona A., D'Elía J., and Paquay S. BEM for the analysis of fluid flow around

MEMS. In S.A. Elaskar, E.A. Pilotta, and G.A. Torres, editors, *Mecánica Computacional, vol. XXIV*, pages 1104–1119. Córdoba, Argentina, 2007.

Kim S. and Karrila S.J. Integral equations of second kind for Stokes flow: direct solutions for physical variables and removal of inherent accuracy limitations. *Chem. Eng. Comm.*, 82:123–161, 1989.

Kozlov V., Maz'ia V.G., and Rossmann J. *Spectral problems associated with corner singularities of solutions to elliptic equations*. AMS Bookstore, 2001.

Ladyzhenskaya O. *The Mathematical Theory of Viscous Incompressible Flow*. Gordon and Breach Science Publishers, 2 edition, 1969.

Méndez C., Paquay S., Klapka I., and Raskin J.P. Effect of geometrical nonlinearity on MEMS thermoelastic damping. *Nonlinear Analysis: Real World Applications*, 10(3):1579–1588, 2008.

Mikhlin S.G. *Multidimensional Singular Integrals and Integral Equations*. Pergamon Press, 1965.

Mikhlin S.G. *Mathematical Physics, An Advanced Course*. North-Holland, 1970.

Mustakis I. and Kim S. Microhydrodynamics of sharp corners and edges: traction singularities. *AIChE Journal*, 44(7):1469–1483, 1998.

Paquay S. *Développement d'une méthodologie de simulation numérique pour les problèmes vibro-acoustiques couplés intérieurs/extérieurs de grandes taille*. Ph.D. thesis, Faculté des Sciences Appliquées, Liège, 2002.

Power H. and Miranda G. Second kind integral equation formulation of stokes flows past a particle of arbitrary shape. *SIAM J. Appl. Math.*, 47(4):689–698, 1987.

Power H. and Wrobel L. *Boundary Integral Methods in Fluid Mechanics*. Computational Mechanics Publications, Southampton,UK, 1995.

Pozrikidis C. *Introduction to Theoretical and Computational Fluid Dynamics*. Oxford, 1996.

Pozrikidis C. *Boundary Integral and Singularity Methods for Linearized Viscous Flow*. Cambridge University Press, 1997.

Sonzogni V., Yommi A., Nigro N., and Storti M. CFD finite element parallel computations on a beowulf cluster. In *ECCOMAS 2000*. 2000.

Storti M., D'Elía J., and Idelsohn S. Algebraic Discrete Non-Local (DNL) absorbing boundary condition for the ship wave resistance problem. *J. Comp. Physics*, 146(2):570–602, 1998a.

Storti M., D'Elía J., and Idelsohn S. Computing ship wave resistance from wave amplitude with the DNL absorbing boundary condition. *Comm. Numer. Meth. Engng.*, 14:997–1012, 1998b.

Storti M.A. and D'Elía J. Added mass of an oscillating hemisphere at very-low and very-high frequencies. *ASME, Journal of Fluids Engineering*, 126(6):1048–1053, 2004.

Taylor D.J. Accurate and efficient numerical integration of weakly singulars integrals in Galerkin IFIE solutions. *IEEE Trans. on Antennas and Propagation*, 51(7):1630–1637, 2003a.

Taylor D.J. Errata to "Accurate and efficient numerical integration of weakly singulars integrals in Galerkin IFIE solutions". *IEEE Trans. on Antennas and Propagation*, 51(9):2543–2543, 2003b.

Tezduyar T., Mittal S., Ray S., and Shih R. Incompressible flow computations with stabilized bilinear and linear equal order interpolation velocity-pressure elements. *Comp. Meth. App. Mech. Engng.*, 95:221–242, 1992.

Wang X. *Fast Stokes: A Fast 3-D Fluid Simulation Program for Micro-Electro-Mechanical Systems*. Ph.D. thesis, MIT, 2002.